

## Material properties of LPCVD processed n-type polysilicon passivating contacts and its application in PERPoly industrial bifacial solar cells

Stodolny, Maciej K.; Anker, John; Geerligs, Bart L.J.; Janssen, Gaby J.M.; Van De Loo, Bas W.H.; Melskens, Jimmy; Santbergen, Rudi; Isabella, Olindo; Schmitz, Jurriaan; Lenes, Martijn

**DOI**

[10.1016/j.egypro.2017.09.250](https://doi.org/10.1016/j.egypro.2017.09.250)

**Publication date**

2017

**Document Version**

Final published version

**Published in**

Energy Procedia

**Citation (APA)**

Stodolny, M. K., Anker, J., Geerligs, B. L. J., Janssen, G. J. M., Van De Loo, B. W. H., Melskens, J., Santbergen, R., Isabella, O., Schmitz, J., Lenes, M., Luchies, J. M., Kessels, W. M. M., & Romijn, I. (2017). Material properties of LPCVD processed n-type polysilicon passivating contacts and its application in PERPoly industrial bifacial solar cells. *Energy Procedia*, 124, 635-642. <https://doi.org/10.1016/j.egypro.2017.09.250>

**Important note**

To cite this publication, please use the final published version (if applicable). Please check the document version above.

**Copyright**

Other than for strictly personal use, it is not permitted to download, forward or distribute the text or part of it, without the consent of the author(s) and/or copyright holder(s), unless the work is under an open content license such as Creative Commons.

**Takedown policy**

Please contact us and provide details if you believe this document breaches copyrights. We will remove access to the work immediately and investigate your claim.



7<sup>th</sup> International Conference on Silicon Photovoltaics, SiliconPV 2017

## Material properties of LPCVD processed n-type polysilicon passivating contacts and its application in PERPoly industrial bifacial solar cells

Maciej K. Stodolny<sup>a</sup>, John Anker<sup>a</sup>, Bart L.J. Geerligs<sup>a</sup>, Gaby J.M. Janssen<sup>a</sup>,  
Bas W.H. van de Loo<sup>b</sup>, Jimmy Melskens<sup>b</sup>, Rudi Santbergen<sup>c</sup>, Olindo Isabella<sup>c</sup>, Jurriaan  
Schmitz<sup>d</sup>, Martijn Lenes<sup>e</sup>, Jan-Marc Luchies<sup>e</sup>, Wilhelmus M.M. Kessels<sup>b</sup>, Ingrid Romijn<sup>a</sup>

<sup>a</sup>ECN Solar Energy, Westerduinweg 3, 1755 LE Petten, the Netherlands

<sup>b</sup>Eindhoven University of Technology, P.O. Box 513, 5600 MB Eindhoven, The Netherlands

<sup>c</sup>Delft University of Technology, Mekelweg 4, 2628 CD Delft, The Netherlands

<sup>d</sup>MESA+ Institute for Nanotechnology, University of Twente, P.O. Box 217, 7500 AE Enschede, The Netherlands

<sup>e</sup>Tempres Systems, Radeweg 31, 8171 MD Vaassen, The Netherlands

---

### Abstract

We present a detailed material study of  $n^+$ -type polysilicon (polySi) and its application as a carrier selective rear contact in a bifacial  $n$ -type solar cell comprising fire-through screen-printed metallization and 6" Cz wafers. The cells were manufactured with low-cost industrial process steps yielding  $V_{oc}$ s from 676 to 683 mV and  $J_{sc}$ s above 39.4 mA/cm<sup>2</sup> indicating an efficiency potential of 22%. The aim of this study is to understand which material properties determine the performance of POCl<sub>3</sub>-diffused ( $n$ -type) polySi-based passivating contacts and to find routes to improve its use for industrial PERPoly (Passivated Emitter Rear PolySi) cells from the point of view of throughput, performance, and bifacial application. This paper reports on correlations between the parameters used for low pressure chemical vapour deposition (LPCVD), annealing, and doping on optical, structural, and electronic properties of the polySi-based passivating contact and the subsequent influence on the solar cell parameters.

© 2017 The Authors. Published by Elsevier Ltd.

Peer review by the scientific conference committee of SiliconPV 2017 under responsibility of PSE AG.

**Keywords:** Polysilicon; Passivating contact; Carrier selective contact; LPCVD; industrial n-type solar cell; Bifacial

---

## 1. Introduction

The performance of current industrial solar cells is limited by recombination at the metallic contacts and recombination at the surface regions with doped layers. A solution to overcome this is to use so-called carrier-selective contacts [1]. The combination of a tunnel oxide and doped polysilicon (polySi) was demonstrated in the 1980s to be a viable candidate for the creation of such passivating contact [2,3]. Recent progress on such devices, achieving conversion efficiencies above 25% on small area lab cells [4,5] and up to 21% on 6" bifacial cells [6,7] merits further investigation and effort for higher efficiencies and towards industrialization of this concept.

The aim of this study is to understand which polySi processes and polySi/SiO<sub>x</sub>/Cz-Si interface parameters determine the performance of polySi passivating contacts made by low pressure chemical vapour deposition (LPCVD) that are implemented in PERPoly (Passivated Emitter Rear PolySi) cells as depicted in Fig. 1. This paper reports on correlations between LPCVD deposition, annealing and doping parameters on optical, structural, and electronic properties of the polySi. The formation of the tunnel oxide was also varied. The aim is to find routes to improve passivation quality and the majority carrier transport (both laterally in the polySi as well as through the oxide) of rear polySi contacts from the point of view of throughput, high efficiency and bifacial application of industrial PERPoly cells resulting in enhanced annual energy output.

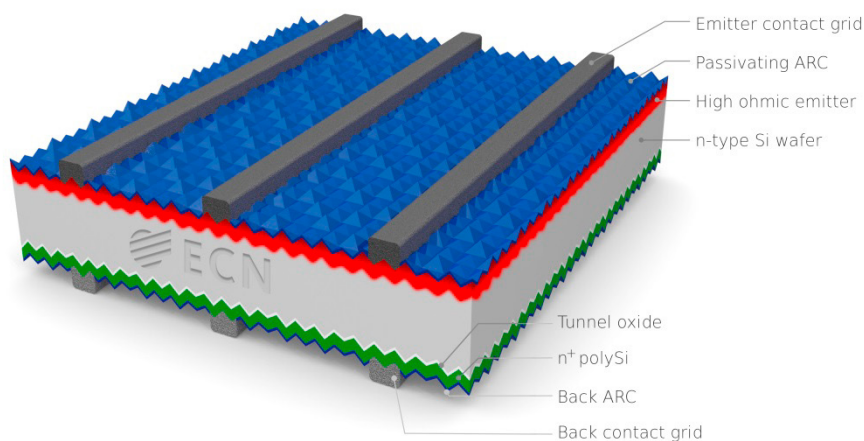


Fig. 1.  $n^+$ -doped polysilicon applied as a rear contact in a bifacial n-type PERPoly (Passivated Emitter Rear PolySi) solar cell comprising fire-through screen-printed metallization and 6" Cz wafers.

## 2. Materials and methods

### 2.1. Experimental approach

In this work we systematically studied the polySi layers that were produced in a high-throughput industrial LPCVD furnace and were subsequently doped by means of POCl<sub>3</sub> diffusion. The effect of variations of process steps and physical properties of the polysilicon structures on  $iV_{oc}$  was characterized via lifetime measurements, and related to the dopant profile measured by electrochemical capacitance-voltage (ECV) profiling and secondary ion mass spectrometry (SIMS). A wide variation of polysilicon layers was tested in n-type bifacial PERPoly cells with a front-diffused boron emitter and rear n-type polySi, with screen-print fire-through metallization on both sides as described in our previous work [7]. The work is compatible with current industrial n-type technology.

### 2.2. Sample definition

Symmetrical samples (same surface properties on both sides) were fabricated on commercially available 5  $\Omega\text{cm}$  n-type 6" Czochralski (Cz) wafers. The thickness of chemically polished wafers was  $\sim 160$   $\mu\text{m}$  and of textured wafers  $\sim 165$   $\mu\text{m}$ . On top of a thin oxide that was grown thermally (Th.Ox) at the temperature of polySi deposition, an intrinsic polySi layer was deposited with varying deposition parameters, such as temperature, silane (SiH<sub>4</sub>) flow,

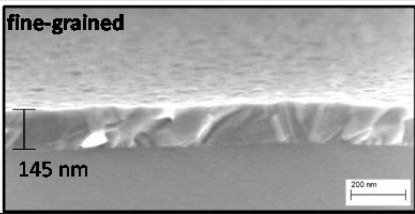
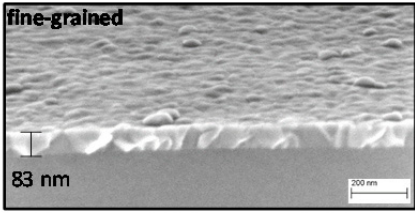
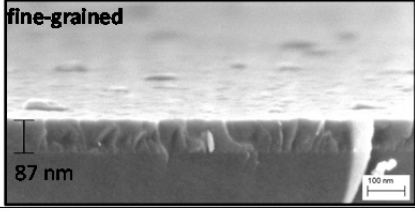
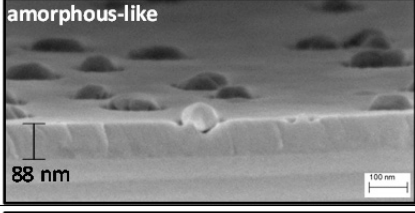
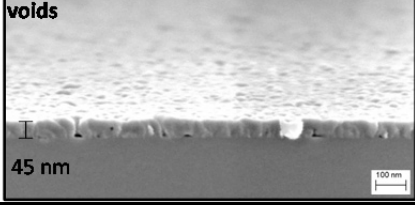
and pressure (the deposition time was kept constant). Subsequently, polySi layers were doped with phosphorus (P) by means of a standard  $\text{POCl}_3$  diffusion at 850 °C [7].

### 3. Results and discussion

#### 3.1. PolySi structural properties

Table I shows the LPCVD parameters that were varied to obtain different growth rates and morphologies of the polySi layers. The growth rate increased for higher temperatures and for higher  $\text{SiH}_4$  flow rates. In particular, the product of temperature and  $\text{SiH}_4$  flow ( $T \cdot \text{flow}$ ) is strongly (and linearly) correlated with the growth rate in the investigated growth regime. The morphology of the polySi layer was significantly influenced by the growth temperature. Fine-grained polySi layers, which were columnar and pinhole-free, were obtained at temperatures above 595 °C. At a lower temperature of 580 °C, amorphous-like smooth layers with crystalline precipitates (visible for polySi type D, see Table 1) were formed, as was also confirmed by Raman spectroscopy. These morphological differences were also illustrated by RMS roughness measurements obtained with AFM, indicating a roughness i.e.  $\sigma_{\text{RMS}} \approx 3\%$  of the layer thickness for fine-grained polySi layers and  $\sigma_{\text{RMS}} \approx 1.8\%$  for a-Si like layers. For thin polySi layers grown at a lower temperature and a low flow a void formation was observed.

Table 1. LPCVD parameters of polySi layers. Images and layer thickness were obtained with HR SEM.

SEM after $\text{POCl}_3$ and phosphosilicate glass removal	
<b>A</b> 610°C high flow	<b>fine-grained</b>  145 nm 200 nm
<b>B</b> 610°C low flow	<b>fine-grained</b>  83 nm 200 nm
<b>C</b> 595°C medium flow	<b>fine-grained</b>  87 nm 100 nm
<b>D</b> 580°C high flow	<b>amorphous-like</b>  88 nm 100 nm
<b>E</b> 580°C low flow	<b>voids</b>  45 nm 100 nm

### 3.2. PolySi electronic properties

Fig. 2a. shows the active P concentration profiles across polySi/SiO<sub>x</sub>/Cz-Si after the same POCl<sub>3</sub> diffusion applied to all layers, measured with ECV analysis. The doping profiles show a correlation between the SiO<sub>x</sub>/polySi deposition parameters and a penetration of P through the interfacial Th.Ox. This penetration shows a significant correlation with the performance of the polySi contact by lowering the contact resistivity while maintaining selectivity [4], in agreement with modeling studies [8]. SiO<sub>x</sub>/polySi layers grown at the highest temperatures (A, B) showed a sharp cut-off of active P-doping at the Th.Ox location while a moderate ‘penetrating diffusion’ profile was observed for SiO<sub>x</sub>/polySi layers deposited at lower temperatures (C, D). For very thin polySi layers with voids (E), the dopant diffused more significantly into the c-Si base.

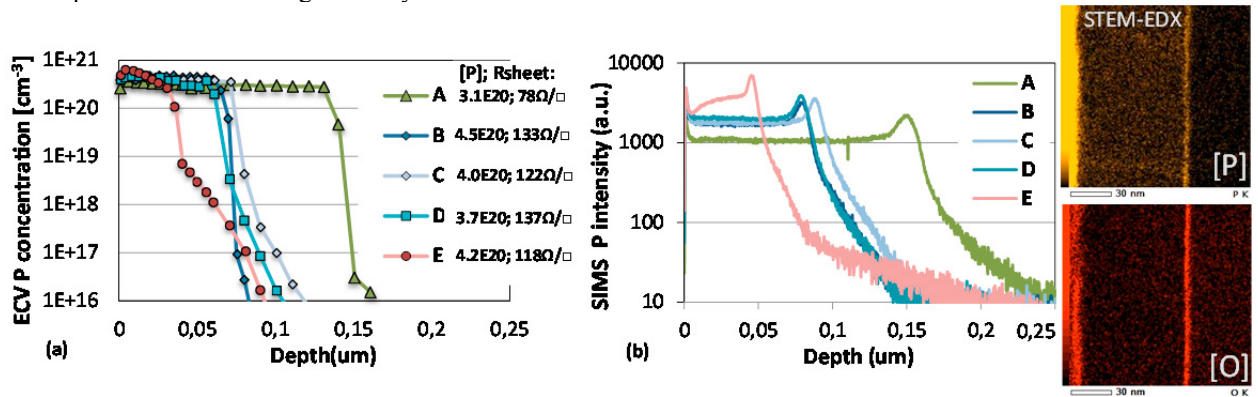


Fig. 2. (a) ECV and (b) SIMS of P doping profiles of investigated polySi/SiO<sub>x</sub>/Cz-Si structures with the corresponding  $R_{\text{sheet}}$  values. (c) STEM-EDX mappings of P and oxygen across polySi type B.

Fig. 2b. shows the total P doping profiles of the same samples, as measured with SIMS. The noticeable difference compared to the active P profiles (ECV, Fig. 2a) is that inactive P accumulated in close vicinity to the Th.Ox. This is confirmed by STEM-EDX mappings of phosphorus and oxygen across the polySi/SiO<sub>x</sub>/Cz-Si structure (Fig. 2c). The interfacial SiO<sub>x</sub> acts thus well as a dopant barrier (ECV/SIMS), while still allowing a certain degree of dopant penetration, and accumulates inactive P (SIMS/STEM-EDX).

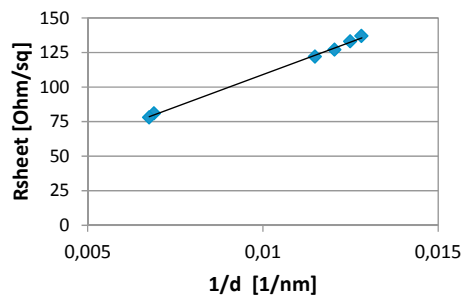


Fig. 3. Sheet resistance as a function of inverse thickness of the layers.

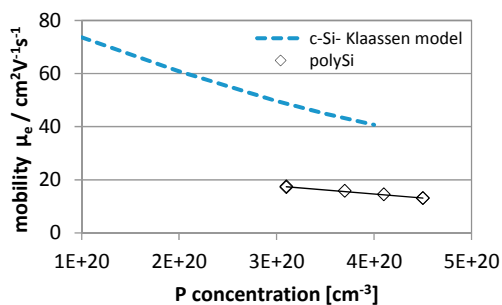


Fig. 4. Mobility in polySi layers as a function of P concentration from ECV, compared to mobility of doped monocrystalline Si.

### 3.3. PolySi passivation properties

Fig. 5 shows the the recombination current  $J_0$  of  $n$ -polySi/SiO<sub>x</sub> structures, with varying polysilicon thickness, as a function of the phosphorus concentration. The closed symbols show the  $J_0$  of doped polySi layers that were partially hydrogenated during cooldown in air after POCl<sub>3</sub> diffusion without a specific later hydrogenation process such as by deposition of SiN<sub>x</sub>. The  $J_0$  decreases with higher doping concentration, which can be attributed to enhanced field-effect passivation. Applying SiN<sub>x</sub> resulted in large reduction in  $J_0$  (open symbols) – in particular for the textured samples (red open symbols), which can be attributed to increased chemical passivation due to full hydrogenation of the interface defect states. The improvement in  $J_0$  was more significant on textured samples (red symbols) with respect to planar samples (blue symbols), possibly due to the higher amount of interface state defects that could be hydrogenated in case of the textured samples.

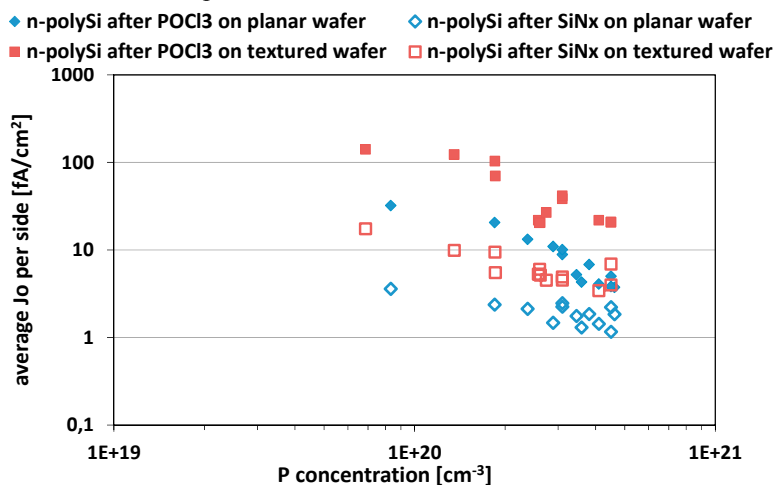


Fig. 5.  $J_0$  from lifetime measurements (Sinton WCT120) after POCl<sub>3</sub> doping (closed symbols) and after SiN<sub>x</sub> (open symbols) versus the P concentration in the polySi. All  $J_0$  values are averages, of up to 15 points on 3 wafers.

Fig. 6. shows the modelling results of  $n$ -polySi passivation properties (expressed by the recombination current  $J_0$ ) with various doping levels as a function of surface recombination velocity ( $S$ ) of the silicon wafer at the interface with the oxide/polySi stack. When comparing Fig. 5 with Fig. 6, a good agreement between experimental and modelling data can be observed. Fig. 6 shows that the  $J_0$  is mainly determined by the  $S$ , and in second order the field effect (P concentration). Hydrogenation reduces the  $S$  by a factor of about 3. Also the observation that the  $S$  values between textured and planar samples differ by another factor of about 3 corroborates that the surface enhancement is about 1.7, and there is another enhancement because of the orientation of the crystal planes.

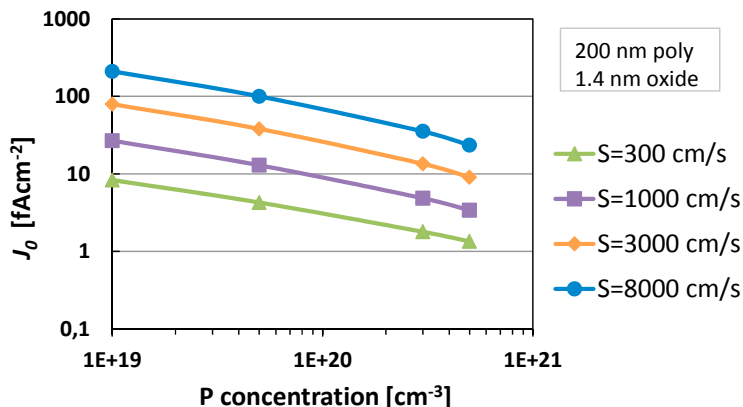


Fig. 6. Modelled  $J_0$  of n-polySi with various doping levels as a function of surface recombination velocity.

### 3.4. Application of polySi in industrial bifacial n-type cells

Several polySi layers were implemented as a rear polySi passivating contact in industrial PERPoly cells processed as described in [7]. These SiO<sub>x</sub>/polySi layers selected for cell level investigation were type A-C and E with Th.Ox as described above, and type B\*=B-with-NAOS (nitric acid oxidized silicon surface; a more leaky, pinhole-rich, chemical oxide as reported in [7]). The polySi layers were deposited with a nominal thickness of 100 nm and 200 nm. Fig. 7 shows the active P concentration profiles in the polySi layers after the same POCl<sub>3</sub> diffusion was applied to all layers, measured with ECV analysis. The P in-diffusion behavior described in Section 3.2 is similarly observed here. However, the active P concentration for thicker layers was reduced due to a rate-limited supply of phosphorus from the phosphosilicate glass. Comparing layers B and B\* (where interfacial SiO<sub>x</sub> was varied) an even further reduction of the active P-concentration was observed. In fact, the integral density of P in the ECV profiles (per unit area) is not constant over the profiles, but generally decreases as the tails become more prominent. The reason for this is not clear. The increased in-diffusion of Ph in profiles B and B\* could be explained by the barrier properties of Th.Ox versus NAOS with the latter known to have pinholes promoting leakage [9].

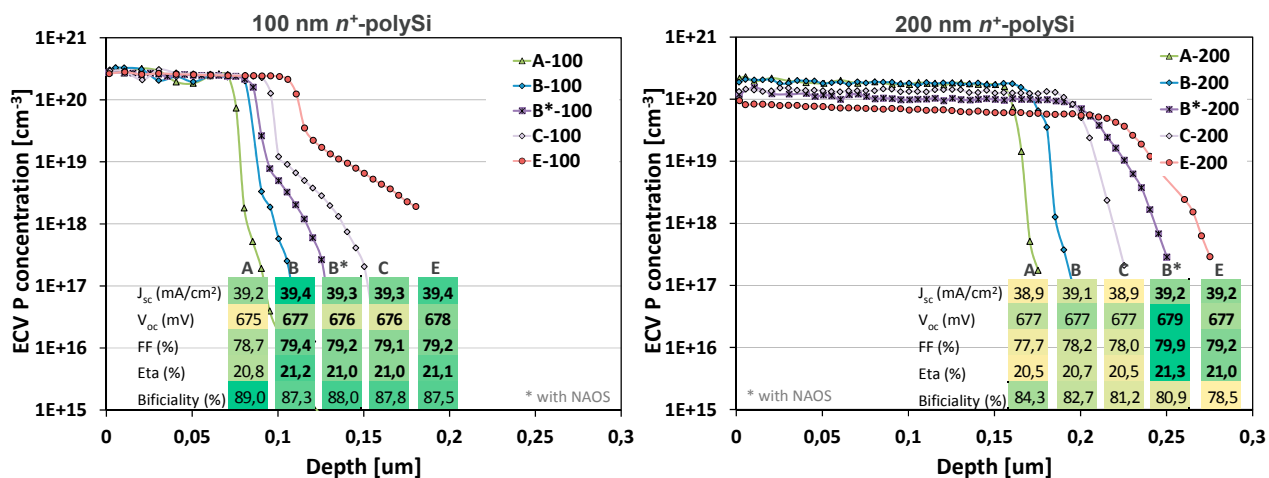


Fig. 7. ECV of P doping profiles of investigated polySi/SiO<sub>x</sub>/Cz-Si structures and the corresponding PERPoly cell results utilizing such polySi layers.

Fig. 7 also reports for every polySi layer the corresponding best obtained cell results, when the polySi layer was applied as the rear passivating contact, metallized with an industrial fire through paste (efficiency results are spectral

mismatch corrected,  $I_{sc}$  measurement calibrated with FhG ISE certified n-PERT reference cell, measured on AAA Wacom system, in house).

For all cells a very high  $V_{oc}$  was observed, with an average over the different polySi variations of 676 mV, indicating that passivation provided by polySi is not significantly decreased after fire-through metallization, even for thinner polySi layers of 100 nm. In fact the difference in  $V_{oc}$  between the cells with 100 nm and 200 nm polySi layers is only about 1 mV. Compared to  $iV_{oc}$  prior to metallization, a  $V_{oc}$  loss was around 20 mV in all cases for both 100 and 200 nm polySi thickness and was attributed mainly to recombination from the front side contacts on the diffused B-emitter. The contact recombination at the rear metal contact pattern on the PERPoly cells was determined to be low, in the range of 100-200 fA/cm<sup>2</sup>.

A significantly higher  $J_{sc}$  was obtained for cells with the thinner polySi as compared to those with thicker polySi, due to a reduction of free-carrier absorption (FCA) of IR light at the rear side. Spectroscopic ellipsometry and transmission-reflection measurements with parameterization of the FCA indicate that the polySi thickness is the main factor that determines FCA and polySi structural properties only slightly influence the FCA losses. Relatively high  $J_{sc}$  can also be obtained for thicker polySi layers with reduced doping concentration (for B\* and E-type polySi layers). The bifaciality of PERPoly cells is also improved with thinner polySi and reaches 87% (for best front efficiency of 21.2%), compared to 81% for thicker layers (for best front efficiency of 21.3%).

For all cells, the same uniform B-emitter with sheet resistance of 80 Ohm/sq was used, so the observed differences of  $FF$  are controlled by the different polySi layers. It turns out to be beneficial for high  $FF$  is to realize a P-tail starting at the thin oxide and extending the P-doping into the wafer. Such a profile can be obtained e.g. by using a thin heavily doped polySi, for which in our experiments P penetrated through the thermal oxide. In case of using a more “leaky” chemical oxide (NAOS), such a beneficial tail could be obtained with both thin and thick polySi. Amorphous-like polySi deposited at lower temperature (E-type layer) resulted similarly in P in-diffusion. Further investigation is ongoing to check the influence of the junction resistance and the resistivity of the poly/metal contact on the  $FF$ .

The properties of the polySi-based passivating contact significantly influence the efficiency of the PERPoly cells (in total by nearly 1% absolute in this study, ranging from 20.5% to 21.3%). A proper design of the polySi thickness and the P doping profile across the thin oxide is essential for the highest  $J_{sc}$ ,  $FF$  and bifaciality. Further efficiency improvements are possible by increasing  $V_{oc}$  via reducing front-side recombination. In a first follow-up experiment, a polySi layer (B) on the rear has been combined with improved boron emitters (100 ohm/sq, deep emitter profile). A  $V_{oc}$  of 683 mV was obtained, which is a 1% relative increase over the cell with a standard emitter, while keeping the  $J_{sc}$  at the same high level. This route of high performance boron emitter, when it can be combined with an improved  $FF$  above 81%, will result in 22% efficiency 6” PERPoly cells.

#### 4. Summary

The material and electronic properties of  $n^+$  polySi layers have been investigated as a function of LPCVD deposition and doping parameters. Optical, structural, and electronic properties of the deposited LPCVD layers and of the resulting doped polySi significantly influence the passivating quality and the cell performance. Especially the  $J_{sc}$  of PERPoly cell was increased for less doped and thinner polySi layers due to a reduced free-carrier absorption of IR light. The  $FF$  could be strongly improved by a doping profile that penetrated across the interfacial oxide (in-diffusion profile in the wafer), with a wide process window where the in-diffusion benefits  $FF$  but does not harm passivation. This in-diffusion can be tuned by process parameters for oxide growth, LPCVD deposition, as well as POCl<sub>3</sub> diffusion. Moreover, a high and stable  $V_{oc}$  was found for 100 and 200 nm thick polySi which confirms the broad processing window, enabling easy tuning of the other cell parameters. With an industrially diffused uniform boron emitter, and screen-printed fire through pastes for contacting, an efficiency of 21.3%, and  $V_{oc}$  and  $J_{sc}$  values good enough to reach 22% have been demonstrated with these rear  $n^+$  polySi-based passivating contacts.



## Acknowledgments

Part of this work was performed in the project *Antilope* (TEID215011), which receives funding from the Topsector Energie of the Dutch Ministry of Economic Affairs.

Hande Ciftpinar and Kacper Blak are acknowledged for their contribution to this work.

Marcel Verheijen is thanked for the STEM-EDX analyses (Philips Innovation Services).

Mark Smithers<sup>d</sup> is acknowledged for HR-SEM imaging.

## References

- [1] E. Yablonovitch, R. M. Swanson and Y. H. Kwark, Proceedings of the 17<sup>th</sup> IEEE Photovoltaic/Spec. Conf., pp.1146 -1148, 1984.
- [2] G.R. Wolstenholme, N. Jorgensen, P. Ashburn, and G.R. Booker, J. Appl. Phys. 61, 225 (1987).
- [3] J.Y. Gan and R.M. Swanson, 21<sup>st</sup> IEEE Photovoltaic Specialists Conference, Vol. 1, pp. 245-250, 1990.
- [4] H. Steinkemper, F. Feldmann, M. Bivour and M. Hermle, IEEE Journal of Photovoltaics, Vol. 5, NO.5, pp.1348-1356, 2015.
- [5] S. W. Glunz, F. Feldmann, A. Richter, M. Bivour, C. Reichel, H. Steinkemper, J. Benick, M. Hermle, 31st European Photovoltaic Solar Energy Conference and Exhibition, September 2015, Hamburg.
- [6] Y. Tao, V. Upadhyaya, C.-W. Chen, A. Payne, E.L. Chang, A. Upadhyaya, A. Rohatgi, Prog. Photovolt.: Res. Appl. (2016), <http://dx.doi.org/10.1002/pip.2739>.
- [7] M.K. Stodolny, M. Lenes, Y. Wu, G.J.M. Janssen, I.G. Romijn, J.R.M. Luchies, L.J. Geerligs, Solar Energy Materials and Solar Cells, Volume 158, Part 1, Pages 24-28.
- [8] G.J.M. Janssen, et al., submitted for publication.
- [9] T. F. Wietler, D. Tetzlaff, J. Krügener, M. Rienäcker, F. Haase, Y. Larionova, R. Brendel, and R. Peibst, Applied Physics Letters 110(25):253902